

Geochemistry of the Shales of the Eccca Group, Karoo Supergroup in the Borehole KZF-1: Implications for Provenance, Paleoweathering and Tectonic Setting

*Tsibula J Sekantsi**, Mahlatse M Ntake, Ronaldo Malapana, Sibusiso Maseko, Mokgadi K Teffo and Christopher Baiyegunhi

Department of Geology and Mining, University of Limpopo, Private Bag X1106, Sovenga 0727, Limpopo Province, South Africa

Received May 24, 2023; Accepted July 20, 2023

Abstract

The Main Karoo Supergroup, situated in South Africa is one of the most unique basins to ever be discovered since it has the thickest and most complete stratigraphic sequences, from the Permo-Carboniferous to the Jurassic age. Despite the fact that the targeted hydrocarbon exploration in the region is hosted in the Eccca Group, little attention is focused on the study of provenance in this region. As a result, this study attempt to use the geology and geochemistry of the Eccca Group shales to unravel the provenance, paleoweathering conditions and tectonic setting of the area. Thirty representative shales of the Eccca Group in borehole KZF-1 underwent geochemical analysis involving major and trace element. The provenance discrimination diagrams based on major oxide geochemistry revealed that the shales are mainly of quartzose sedimentary and mafic igneous provenances. The bivariate plots of TiO_2 versus Zr, La/Th versus Hf and ternary diagram of V-Ni-Th $\times 10$ suggest that the shales were derived from mafic igneous rocks. The tectonic setting discrimination diagrams support active-passive continental margin setting of the provenance. Chemical index of alteration (CIA) indices and the bivariate plot of SiO_2 against total alkali ($Al_2O_3+K_2O+Na_2O$) suggest that the shales have underwent intense degree of chemical weathering under arid climate.

Keywords: *Geochemistry; Oxides, elements; Eccca Group; Karoo Supergroup.*

1. Introduction

The Karoo Supergroup in South Africa is said to cover an extensive area, the Main Karoo Basin, the Kalahari Basin, and several other subsidiary basins in Namibia, Botswana, Mozambique, Zimbabwe, and South Africa [1]. The author added that the Main Karoo Basin covers approximately 300 000 km² and it is a clear representation of about 100 million years of deposition which began in the late Carboniferous throughout Gondwana and ended in the Middle Jurassic when the supercontinent Gondwana broke up [2]. A shale is classified as a clastic sedimentary rock that formed from a combination of mud, clay, and tiny fragments of other minerals such as quartz and calcites. It normally consists of very fine-grained material, which split easily or is regarded as being fissile after it has been consolidated and lithified into a rock [1-4]. Additionally, this is normally deposited in a calm environment such as a deep sea or deep marine and even lakes. Geochemistry can be characterized as the study that involves chemical principles or the distribution and occurrence of chemical elements in the earth to give a deeper understanding of the earth and other planets' systems. It is of major importance, especially in the process of mineral concentration, be it by weathering agents, hydrothermal, magmatic, metamorphic, hydraulic, or even a combination of these processes [3]. It is useful in the exploration of geothermal resources during surface exploration and after exploration wells have been drilled and discharged [4].

Essentially, fine-grained materials such as shales are highly bombarded with trace elements with some of these elements being immobile (like Th, Hf, Sc, rare earth elements (REE), and Zr) and they are also homogeneous be it pre-deposition or post-deposition [5]. Furthermore, these

are observed to have very low concentrations in natural water but are transported almost infinitely from their parent rocks to their depositional environments. Their distribution in felsic and in mafic rocks differ in the sense that there is normally a high concentration of La and Th in felsic rocks while there is a high concentration of Sc, Cr, and Co in mafic rocks [5]. While another author added that the above-mentioned elements are regarded as being immobile during weathering processes hence the availability of lithic material consisting of these elements can reveal the composition of the source rock, since they are a sensitive indicator, especially when considering the ratios of La or Th to Co, Sc, or Cr [6-8]. The same ideology can be applied when looking at REE such as Eu, which is normally preserved in fine-grained material [6]. According to [5], it has been found that felsic rocks tend to have a negative Eu anomaly (Eu/Eu^* from chondrite-normalized plots of the REE) while there seems to be a low to no Eu anomaly in basic rocks. [5] went further to explain that other elements like major elements are regarded as mobile, meaning their mobility makes them sensitive to climatic changes hence they can be used to determine the climatic evolution of the palaeoenvironment. The shale in the Ecca Group is characterized by having a higher concentration of Fe_2O_3 , K_2O , TiO_2 , Ce, Cu, Ga, La, Nb, Nd, Rb, Sc, Sr, Th, and Y [6]. One of the reasons for the sudden fascination with the shale within the Ecca Group is due to the presents of the natural resources trapped deep within the shales of the Karoo. Which covers an area of about 155 000 km^2 when considering the thinning of the Karoo to the north [2,7].

There have been several studies conducted around trying to assess the chemical differences and compositional variations of some shales and sandstones by the likes of [5] and [6]. This would help create a better understanding of how sedimentary processes and composition of the provenance plays a role in the different shales available. There is a lack of understanding as to how local variability of the composition of shales and sandstones compare to regional variation in their composition. While other researchers [1-7] have gone on to evaluate and come up with geochemical investigations that relate to the provenance and tectonic evolution of sedimentary basins, however not much clarity has been given to such factors, especially that of the Ecca Group [5-7]. Also remembering how important the tectonic evolution of the Karoo Basin shaped the depositional environment. Geochemical studies on the fine-grained material of the Ecca Group in the Western Cape have not been done in detail especially when it comes to determining their source rock characteristics of the tectonic setting and the provenance. As such the purpose of this study is to account for the geochemistry and geology of the Ecca Group shales and investigate their implications on the provenance, tectonic settings, and weathering process. The study area is situated within the Karoo Basin in the Western Cape Province in Tankwa Karoo Sub-basin at a latitude of $32^\circ 50' 30.43''$ S and a longitude of $19^\circ 44' 33.02''$ E, with the actual drill hole being the KZF-1 within the Main Karoo as depicted in Figure 1, demarcated with a red star [15].

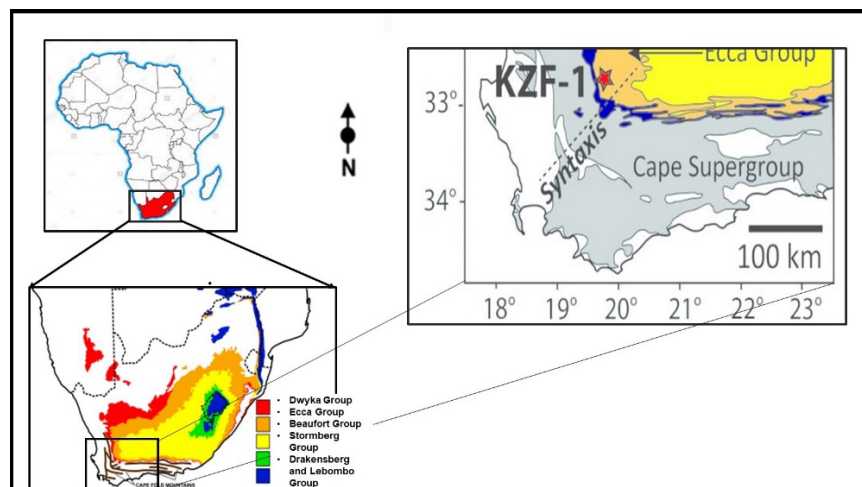


Figure 1. Geological map of the Main Karoo Basin (modified from [8])

2. Geological setting

The Main Karoo Supergroup is bound by the Cape Fold Belt in the southern portion of Gondwana and the northern portion by the Kaapvaal Craton or rather the Cargonian highland (Figure 2). This is due to a shallow angle subduction of the paleo-Pacific plate beneath the Gondwana Supercontinent-within a foreland trough. This resulted in the formation of a wide-fold-thrust belt which is called the Cape Fold Mountain [7]. However, there have been several other theories that have been brought forward that relate to the formation of this basin, with some authors such as [9] agreeing that it may have formed in response to a flexure foreland basin to the Cape Fold Belt. While some believe it may have been a result of a trans-tensional foreland system formed by subsistence and tilting in a strike-slip scenario or from a thin-skinned fold belt that occurred during tectonic movements that resulted in collisions or from an extensional back-arc basin that occurred because of an oblique subduction of the Palaeo-Pacific plate below the western Gondwana [10].

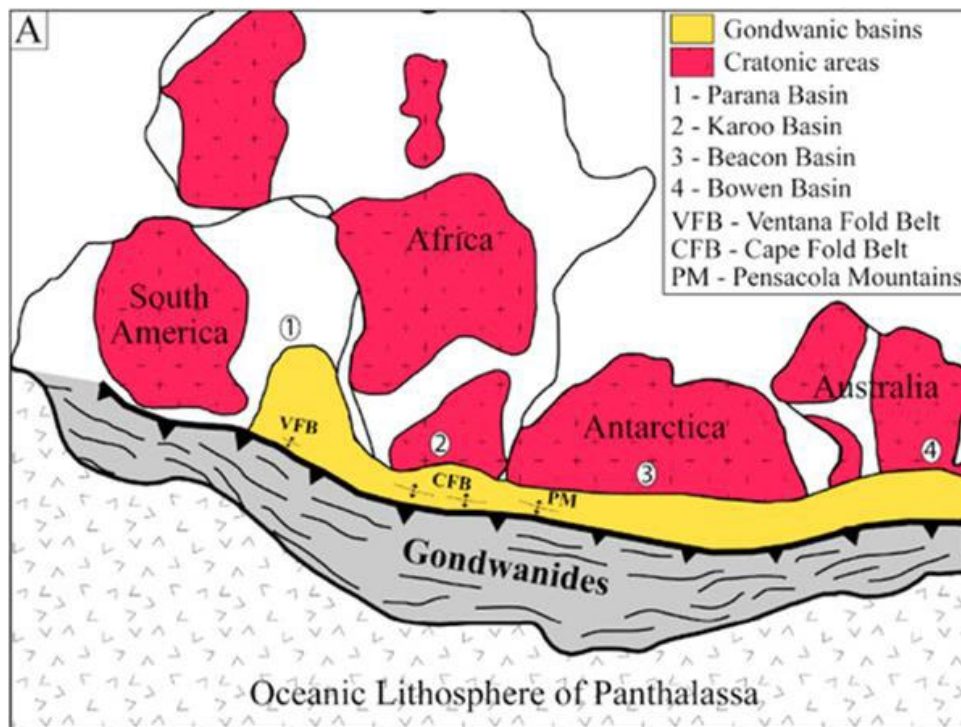


Figure 2. Map showing the Gondwanic basins and cratonic areas of Gondwana (adapted from [14])

The Karoo Supergroup rocks are deposited conformably above the Cape Supergroup, while in the Northern portion, they are unconformably resting above the Achaean Kaapvaal Craton as suggested by [9]. The author further added that the sedimentation emphasizes a change in environmental conditions from glacial to marine, deltaic, fluvial, and lastly aeolian. Gondwana is a Supercontinent that formed during a collisional event that resulted in Africa, South America, India, Antarctica, and Madagascar being joined together hence perpetuating the formation of the Karoo Supergroup as depicted in Figure 2. Scientists believe that there was a development of a shallow angle subduction of the Palaeo-Pacific plate beneath the Supercontinent which caused an upliftment hence the mountain build-up (orogenesis) further south.

This event resulted in an approximately 12 km thick succession of sedimentation occurring within a large intra-cratonic retro-arc foreland basin in the south-western portion of Gondwana [6]. There was a time of uplift and erosion following the deposition of the Cape Supergroup in the pre-Karoo basin. A significant ice sheet covered the early Karoo basin and the nearby mountains while the southern portion of Gondwana migrated across the South Pole. The basal Karoo Dwyka Formation is a product of glacial sedimentation in both the upland valley and shelf

deposits [11]. The author further added that after the glaciation, a vast shallow sea persisted over the shelf that was gradually sinking, nourished by copious amounts of melt water. The peculiar Mesosaurus-bearing, carbonaceous shales of the Whitehill Formation were produced during an "interglacial" that may have been warmer than the Lower Ecca, during which black clays and muds accumulated. Thereafter, there was the deposition of the Upper Karoo basin, this sedimentary filling occurred after the basin was exposed to erosion post-Gondwana time, which resulted in a hiatus that also caused the age of the youngest deposit of the Main Karoo to range in age from Triassic to Mid-Jurassic [12]. Throughout the late Triassic and early Jurassic, the upper Karoo sequence's gradual aridification and tectonic deformation of the basin resulted in the accumulation of "red beds," which are understood to be fluvial and flood-fan, playa, and dune complexes, in four different depositories (Elliot Formation) [13]. Over time, this gave way to deposition driven primarily by westerly winds, which clogged the remaining depositories with fine-grained sand dunes. [13] went on to explain that during the early Jurassic, there was basin-wide volcanic activity started during this period and persisted through the early Cretaceous as a precursor to the break-up of Gondwana in the late Jurassic. The Karoo sequence's key stratigraphic units have undergone Palaeo-environmental research, which shows how more regional tectonic basins have an impact on depositional style.

3. Methodology

A total of thirty representative shales collected from borehole KZF-1 (Figure 1) were studied under the petrographic microscope and analysed for the major oxides and trace element concentrations. X-ray fluorescence (XRF) analysis was performed at the Geochemical laboratory in the Department of Geology and Mining, University of Limpopo, South Africa. The rock samples were neatly cleaned and crushed in to smaller sizes using the Braun Chipmunk VD67 jaw crusher. Thereafter, the HERZOG milling machine was used to mill the crushed samples into powdery form of less than 50µm grain size. Pressed pellets were used for the major oxides and trace elements analyses. The pressed pellets were analysed by PANalytical Zetium XRF spectrometer equipped with a 4 kW Rh tube. The milled samples were also dried at 100°C (weight A) and heated at 1000 °C (weight B) for a period of at least 3 hours to oxidize S and Fe²⁺ in order to determine the loss of ignition (LOI). The mathematical expression for the percentage loss on ignition (LOI) is given as:

$$\% \text{ LOI} = \frac{\text{Weight}_A - \text{Weight}_B}{\text{Weight}_A - \text{Weight}_{\text{crucible}}} \times 100$$

The Epsilon software program was used to quantify the oxides and trace elements in the mudrocks and sandstones. Discriminatory binary and ternary plots of the major oxides and trace elements were used for geochemical classification as well as the determination of provenance and tectonic settings. In addition, chemical index of alteration (CIA), chemical index of weathering (CIW), plagioclase index of alteration (PIA) and index compositional variation (ICV) were calculated and bivariate diagram of ICV against CIA and ternary diagram of Al₂O₃–(CaO+Na₂O)–K₂O were plotted to deduce the degree of weathering. In the CIA, CIW, PIA and ICV formulas, CaO* is the amount of CaO added into the silicate fraction of the rocks. In this study, rectification for CaO from the carbonate contribution was not carried out because of the absence of CO₂ value. Hence, the proposed method of [6] was used to calculate the amount of CaO* from the silicate fraction. The method suggested that CaO values should be accepted only if CaO < Na₂O. However, when CaO > Na₂O, it was alleged that the concentration of CaO is the same with that of Na₂O. This procedure provides measure for the ratio of the secondary aluminous mineral to feldspar, and forms a basis for the measure of intensity of weathering.

4. Results

4.1. Stratigraphic column

The main focus of this study is on the Ecca Group of the Karoo Supergroup (Figure 3), which is subdivided into four different formations. The base comprises of Dwyka Group with a thickness of 23 m, consisting of three types of tillite which have been divided in terms of colour

ranging from very light grey at the base, light grey and lastly grey at the top of the succession. This tillite is a glacial deposit consisting of a mixture of fine-grained to coarse-grained material, which may also differ in shape as in angular, elongated and even rounded clasts. With the grey tillite having several grey-greenish tuff horizons and calcite beds. These tillites are overlain by the Ecca Group, specifically the Prince Albert Formation with a thickness of 180 m. This consists of several successions of carbonaceous shale, grey shale, two black shale beddings, an alternating layer of light to dark-coloured beds, banded shale consisting of black carbonaceous shale and dark grey shale, some minor fine-grained sand, several greys to lime greenish tuff horizons. With some calcite, quartz veins, some weathered shale lithologies, black specks and, three breccia units including fold structures a slump structures. This is succeeded by the Whitehill Formation which has a thickness of 47,55 m.

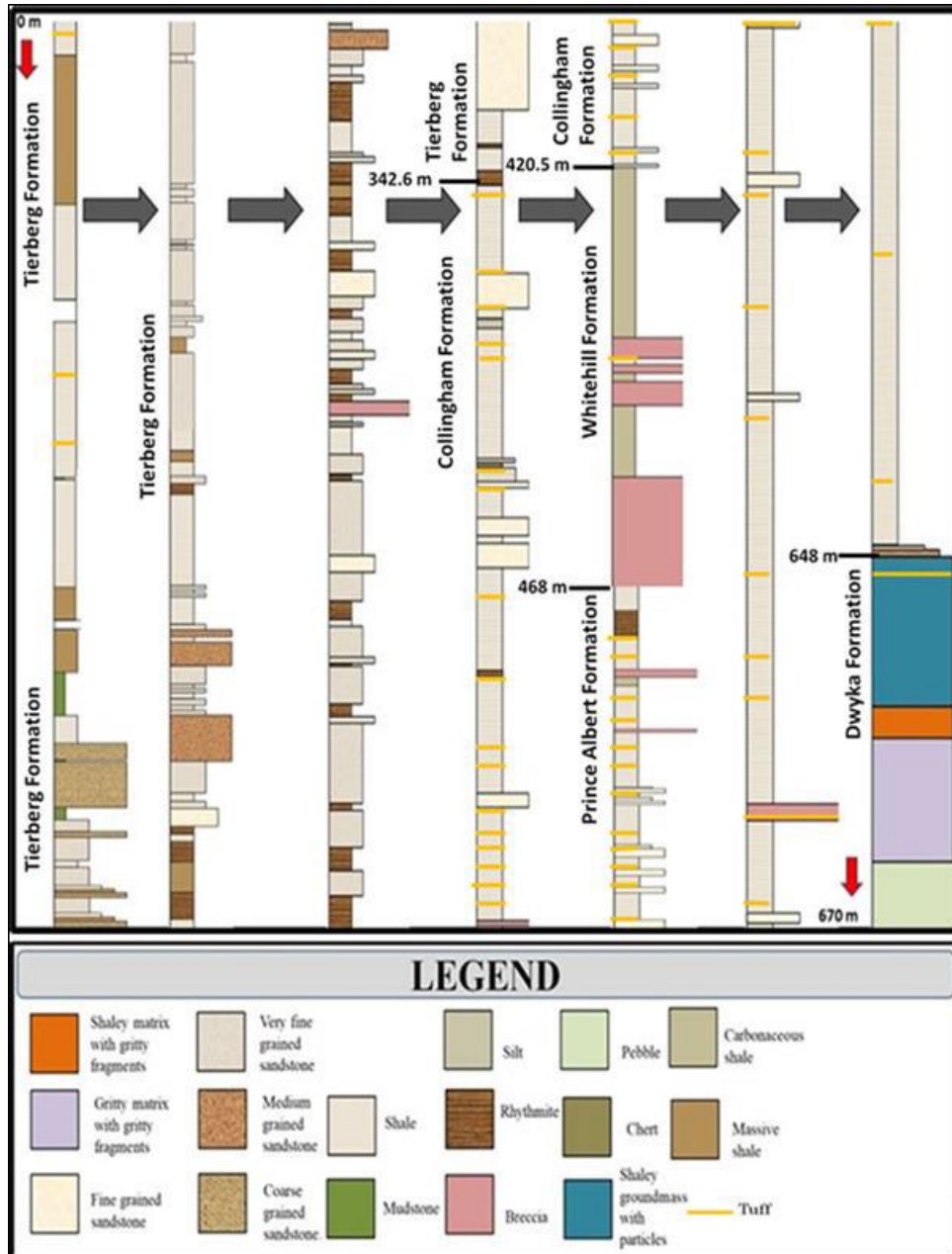


Figure 3. Stratigraphic column of the Karoo Supergroup (the Ecca and Dwyka Group)

They contain several disseminated pyrite inclusions, a vein network of quartz and a calcite bed with structures such as worm structures on the top, some slump structures and massive structures. Followed by the Collingham Formation at 77.90 m consisting of two grey shales, a breccia unit, black shale and lastly a dark grey shale. Some slump structures, several greenish-yellow tuff horizons, several calcite veins, fine-grained sandstone and a single layer of alternating rocks of light and dark shale. Then lastly the Tierberg Formation which has a thickness of 342.55 m, consisting of ten alternating beds of light, dark and whitish grey shale, then layers of dark grey to black shale, seven massive black shales, two light grey shale units and two weathered shale units at the top of the succession. These have minor fine to medium-sized sandstones. Concerning this research, the stratigraphic column is a thickness of 671 m, with it being divided into two main groups. The Dwyka is the oldest and consists of glacial materials such as tillite and the Ecca Group consists mainly of four formations. It is of shale, minor sandstones and, mudstone. These formations are Prince Albert, which is at the base, followed by the Whitehill, then Collingham and lastly the Tierberg Formation at the top.

4.2. Major element composition

Results of the XRF analysis are presented in Table 1, which is found to contain SiO₂ ranging from 48.53-68.45 %, followed by Al₂O₃, Fe₂O₃, and K₂O with their percentages ranging from 14.97-30.67%, 1.89-9.36 % and 2.34-7.51%. The other oxides are Na₂O, MgO, CaO, TiO₂, P₂O₅, and MnO with their percentages ranging from 0,56-2,46%, 0,84- 3,24%, 0,18-3,31, 0,36-0,73%, 0,07-0,26% and 0,01-0,32% showing the lowest percentages, respectively. This table also includes the UCC (Upper Continental Crust) and PAAS (Post Archaean Australian Shale) values from [16-17] in that order. Then there is a loss of ignition and the sum, this calculation is of importance as it helps in confirming the accuracy of the results. The closer the sum is to 100%, the more accurate.

4.3. Trace elements

The trace elements of the Ecca Group are shown in Table 2 below, the results are divided into 3 main groups. The LILE (large ion lithophile elements), HFSE (high field strength elements) and TTE (transition trace elements). The LILE elements consist of Ba, Rb, Sr, Th and U which have a composition ranging from 1559-628 ppm, 84-254.2 ppm, 136.2-320 ppm, 10.5-56.6 ppm and 2.7-17.5 ppm respectively. Then there is Hf, Nb, Zr, Pb and Y with composition ranging from 3.3-16.2 ppm, 10.7-27.3 ppm, 104.8-529.8 ppm, 6.9-64.4 ppm and 21-63.7 ppm respectively and these are classified as HFSE. Lastly the TTE with their composition being 17.3-31.5 ppm, 6-18.2 ppm, 1.4-18.2 ppm, 11-150 ppm, 3.9-71.6 ppm, 34-157 ppm, 1.5-55 ppm and 3.9-71.6 ppm of Ga, Sc, Co, V, Cu, Zn, Ni and Cu respectively. These include their UCC and PAAS values from [17].

4.4. Mineral composition by X-ray diffraction

The X-ray diffraction results are depicted in Table 3. There are seven samples which have been picked in three formations, namely two samples from the Collingham Formation at depths of 377 m and 386 m. Three more samples from the Whitehill Formation at depths of 425 m, 431 m, and 438 m. Then two samples from the Prince Albert Formation at depths of 518 m and 568 m. These seven samples consist of certain percentages of Plagioclase, microcline, quartz, kaolinite, mica, chlorite, smectite, haematite, pyrite, dolomite, garnet, zircon and even zeolite. Tc on the table denotes that they are detected in traces, while the dash represents not detected.

Table 1. Table depicting the major elements of the Eccca Group shales along with its PAAS and UCC values

Depth (m)	Sample ID	Formation	Rock type	SiO ₂ %	Al ₂ O ₃ %	Fe ₂ O ₃ %	MgO%	CaO%	Na ₂ O%	K ₂ O%	TiO ₂ %	P ₂ O ₅ %	MnO%	Cr ₂ O ₃ %	LOI%	Sum of data
14.36	TJ-1	Tierberg	Shale	60,77	15,82	7,65	1,49	1,08	1,70	3,21	0,62	0,21	0,14	0,01	7,10	99,80
55.74	TJ-2	Tierberg	Shale	63,24	15,23	6,80	1,36	1,02	1,59	3,09	0,55	0,20	0,11	0,01	6,60	99,80
113.79	TJ-3	Tierberg	Shale	61,15	17,64	6,44	1,52	0,81	2,09	3,64	0,64	0,20	0,10	0,01	5,50	99,74
164.41	TJ-4	Tierberg	Shale	60,42	16,13	7,28	1,40	1,02	2,12	3,21	0,61	0,14	0,16	0,01	7,30	99,80
189.38	TJ-5	Tierberg	Shale	59,72	15,57	7,96	1,34	1,10	2,02	3,12	0,62	0,25	0,24	0,01	7,80	99,75
231.7	TJ-6	Tierberg	Shale	58,97	16,25	7,27	1,36	1,01	1,87	3,54	0,63	0,22	0,21	0,01	8,40	99,74
275.95	TJ-7	Tierberg	Shale	59,71	15,91	7,56	1,49	1,33	2,28	3,21	0,65	0,19	0,21	0,01	7,20	99,75
279.81	TJ-8	Tierberg	Shale	59,87	16,41	7,33	1,50	0,66	2,11	3,57	0,69	0,15	0,21	0,01	7,30	99,81
299.1	TJ-9	Tierberg	Shale	59,53	16,05	7,57	1,34	0,59	2,36	3,41	0,63	0,17	0,24	0,01	7,90	99,80
323.59	TJ-10	Tierberg	Shale	60,05	15,81	7,24	1,31	0,73	2,50	3,33	0,64	0,15	0,28	0,01	7,70	99,75
376.82	TJ-11	Collingham	Shale	64,57	17,20	3,70	1,15	0,31	2,47	3,67	0,62	0,09	0,04	0,01	5,90	99,73
385.58	TJ-12	Collingham	Shale	61,69	18,51	4,28	1,28	0,64	2,00	4,38	0,68	0,13	0,07	0,01	6,10	99,77
395.8	TJ-13	Collingham	Shale	50,70	27,56	3,17	1,70	0,45	0,59	7,11	0,36	0,09	0,01	0,00	7,90	99,64
398.10	TJ-14	Collingham	Shale	55,75	14,97	9,36	1,55	2,26	1,95	3,39	0,56	1,23	0,32	0,01	8,40	99,75
401.5	TJ-15	Collingham	Shale	50,41	29,00	2,33	1,73	0,26	0,56	7,51	0,36	0,07	0,01	0,00	7,50	99,74
402.1	TJ-16	Collingham	Shale	50,63	28,82	2,47	1,74	0,28	0,59	7,33	0,36	0,10	0,01	0,00	7,40	99,73
424.5	TJ-17	Whitehill	Shale	56,30	16,55	5,94	1,71	1,02	1,69	4,30	0,61	0,26	0,05	0,01	11,30	99,74
428.79	TJ-18	Whitehill	Shale	58,32	15,67	6,22	1,77	0,58	1,67	3,56	0,57	0,19	0,05	0,01	11,20	99,81
431.36	TJ-19	Whitehill	Shale	60,50	15,96	4,54	1,71	0,75	2,28	3,42	0,63	0,17	0,03	0,01	9,80	99,80
431.65	TJ-20	Whitehill	Shale	55,90	16,33	5,04	2,77	2,18	1,95	3,46	0,63	0,20	0,07	0,01	11,20	99,74
434.34	TJ-21	Whitehill	Shale	56,42	16,33	5,94	2,81	1,49	1,52	3,59	0,56	0,15	0,06	0,01	10,90	99,78
438.82	TJ-22	Whitehill	Shale	56,38	16,35	6,81	1,41	0,49	2,03	3,77	0,62	0,16	0,02	0,02	11,70	99,76
458.1	TJ-23	Whitehill	Shale	52,04	17,18	7,13	3,24	3,31	1,53	2,89	0,52	0,21	0,11	0,01	11,60	99,77
488.1	TJ-24	Prince Albert	Shale	53,35	16,28	5,51	1,92	2,51	1,61	3,36	0,62	0,14	0,29	0,01	14,20	99,80
518.1	TJ-25	Prince Albert	Shale	65,41	19,33	2,87	1,01	0,29	1,42	3,62	0,50	0,08	0,03	0,01	5,20	99,77
523.0	TJ-26	Prince Albert	Shale	48,53	30,64	1,89	1,06	0,64	0,87	6,34	0,83	0,17	0,03	0,00	8,60	99,60
540.43	TJ-27	Prince Albert	Shale	61,32	18,29	8,51	1,41	0,20	1,34	2,89	0,64	0,09	0,11	0,01	5,00	99,81
549.08	TJ-28	Prince Albert	Shale	66,53	16,55	6,31	1,08	0,18	1,48	2,55	0,58	0,08	0,09	0,01	4,40	99,84
568.63	TJ-29	Prince Albert	Shale	68,45	16,37	4,72	0,84	0,19	1,72	2,34	0,62	0,07	0,08	0,01	4,40	99,81
611.76	TJ-30	Prince Albert	Shale	64,44	16,98	6,08	1,04	0,20	1,20	2,75	0,73	0,08	0,15	0,01	6,10	99,76
UCC				66,60	15,40	5,04	2,48	3,59	3,27	2,80	0,64	0,12	0,10			
PAAS				62,40	18,78	7,18	2,19	1,29	1,19	3,68	0,99	0,16	0,11			

Table 2. Table depicting the trace elements of the Ecca Group shales along with their UCC and PAAS values

Depth (m)	Sample ID	Formation	Rock type	Ni ppm	Sc ppm	Ba ppm	Be ppm	Co ppm	Cs ppm	Ga ppm	Hf ppm	Nb ppm	Rb ppm	Sn ppm	Sr ppm	Ta ppm	Th ppm	U ppm	V ppm	W ppm	Zr ppm	Y ppm
14.36	TJ-1	Tierberg	Shale	<20	13	685	1	11	11	19	4	12	150	4	164	1	16	4	108	3	166	31
55.74	TJ-2	Tierberg	Shale	<20	12	730	1	15	10	18	5	11	141	3	215	1	15	4	94	3	158	30
113.79	TJ-3	Tierberg	Shale	22	14	817	4	15	10	22	5	12	173	4	200	1	17	5	103	3	166	31
164.41	TJ-4	Tierberg	Shale	<20	14	777	1	12	9	19	5	12	149	4	201	1	18	6	96	2	185	35
189.38	TJ-5	Tierberg	Shale	25	14	773	2	15	10	19	5	12	144	4	211	1	16	5	116	2	181	33
231.7	TJ-6	Tierberg	Shale	21	14	802	<1	11	11	19	5	12	153	4	198	1	17	5	111	2	188	32
275.95	TJ-7	Tierberg	Shale	<20	14	780	<1	14	9	19	6	12	147	4	206	1	17	6	112	3	189	35
279.81	TJ-8	Tierberg	Shale	22	15	802	3	13	10	20	5	12	156	4	169	1	17	6	130	3	179	33
299.1	TJ-9	Tierberg	Shale	<20	14	818	3	16	9	19	5	13	151	4	169	2	18	6	117	3	190	26
323.59	TJ-10	Tierberg	Shale	<20	14	857	2	12	9	18	5	12	144	4	184	1	18	7	122	3	183	35
376.82	TJ-11	Collingham	Shale	<20	15	855	6	11	11	19	5	11	160	4	152	1	18	7	126	3	162	28
385.58	TJ-12	Collingham	Shale	<20	16	1062	3	9	12	21	6	13	179	3	177	1	20	8	125	3	187	35
395.8	TJ-13	Collingham	Shale	<20	7	1002	5	11	23	32	13	24	238	5	296	3	53	17	11	1	443	41
398.10	TJ-14	Collingham	Shale	<20	13	871	1	8	8	17	4	10	142	3	236	1	15	6	112	3	171	31
401.5	TJ-15	Collingham	Shale	<20	6	1321	1	1	13	30	8	16	254	5	280	2	53	13	21	1	211	29
402.1	TJ-16	Collingham	Shale	<20	7	1157	2	3	16	30	7	20	237	5	270	2	51	14	19	1	222	29
424.5	TJ-17	Whitehill	Shale	28	17	823	3	11	11	20	4	12	182	5	169	1	17	5	118	4	131	31
428.79	TJ-18	Whitehill	Shale	37	14	721	2	14	13	18	4	12	163	4	164	1	18	6	96	3	124	24
431.36	TJ-19	Whitehill	Shale	31	13	588	1	9	10	17	3	11	140	4	153	1	16	5	94	2	104	24
431.65	TJ-20	Whitehill	Shale	<20	11	664	3	8	11	18	4	14	149	4	282	1	27	8	90	3	142	24
434.34	TJ-21	Whitehill	Shale	20	13	703	3	10	13	19	5	14	153	4	259	1	18	6	84	4	174	31
438.82	TJ-22	Whitehill	Shale	35	14	696	2	18	11	18	4	13	167	4	158	1	17	4	97	3	135	25
458.1	TJ-23	Whitehill	Shale	<20	14	631	3	5	9	20	6	13	125	3	194	1	20	6	100	3	217	41
488.1	TJ-24	Prince Albert	Shale	36	17	768	1	15	11	18	4	12	157	4	184	1	17	5	115	3	134	24
518.1	TJ-25	Prince Albert	Shale	<20	16	874	3	2	15	21	6	21	178	5	199	1	22	9	73	2	216	47
523.0	TJ-26	Prince Albert	Shale	<20	14	1559	6	5	13	31	16	27	243	6	432	2	56	15	44	5	529	63
540.43	TJ-27	Prince Albert	Shale	29	18	721	4	7	11	21	5	12	153	6	136	1	17	7	121	3	168	34
549.08	TJ-28	Prince Albert	Shale	<20	14	651	3	4	10	19	5	15	135	4	141	1	15	6	89	3	156	31
568.63	TJ-29	Prince Albert	Shale	<20	15	688	2	5	10	17	5	10	121	4	166	1	15	5	93	3	171	30
611.76	TJ-30	Prince Albert	Shale	27	16	684	1	10	10	19	6	14	123	4	148	1	16	7	95	3	196	43
			UCC		14	628		17		17	5	12	84		320		10	3	97		193	21
			PAAS		16	650		23		20	5	19	160		200		14	3	150		210	27

Table 3. X-ray diffraction data with the percentage of minerals contained in the Ecca Group shales

Serial Number	Borehole	Depth (m)	Formation	Plagioclase (%)	Microcline (%)	Quartz (%)	Kaolinite (%)	Chlorite (%)	Mica (%)	Smectite (%)	Illite (%)	Sericite (%)	Hematite (%)	Pyrite (%)	Dolomite (%)	Garnet (%)	Zircon (%)	Zeolite (%)
17	KZF1	377	Collingham	12	4	32	13	10	5	23	-	-	-	tc	-	tc	tc	-
18	KZF1	386	Collingham	13	-	30	11	13	4	28	-	-	-	tc	-	tc	-	-
21	KZF1	425	Whitehill	14	-	23	16	7	17	15	-	tc	tc	7	-	-	-	-
22	KZF1	431	Whitehill	19	-	30	17	10	13	6	-	tc	-	4	-	-	-	-
23	KZF1	438	Whitehill	12	-	32	26	-	2	tc	-	tc	-	5	22	-	-	-
27	KZF1	518	Prince Albert	11	tc	26	12	9	3	33	-	6	tc	tc	-	tc	tc	-
28	KZF1	568	Prince Albert	10	2	25	18	6	3	30	-	5	tc	tc	-	tc	tc	-

where tc- trace concentration and “-“- not detected

5. Interpretation and discussion of results

5.1. Petrography

A shale is a fine-grained rock, which tends to part easily. It looks homogeneous when observed with the naked eye (Figure 4A), but once under the microscope, it is heterogeneous. As shown by Figures 4A to C shales can consist of a variety of colours depending on their source rocks, the type of minerals or elements they contain, the type and amount of organic material or vegetation that was found in that environment and even staining from oxidation.

The brown colour may be a result of clay material. It seems darker than the one shown in Figure 4A, because the clay materials may be in almost equal proportion. While in Figure 4C the clay along with the calcite material might be higher concentration, hence it appears lighter in colour. The mineralogy of the shale includes quartz, clay minerals (e.g., smectite), feldspar, pyrite, carbonate minerals (e.g., calcite) and phosphates [34].

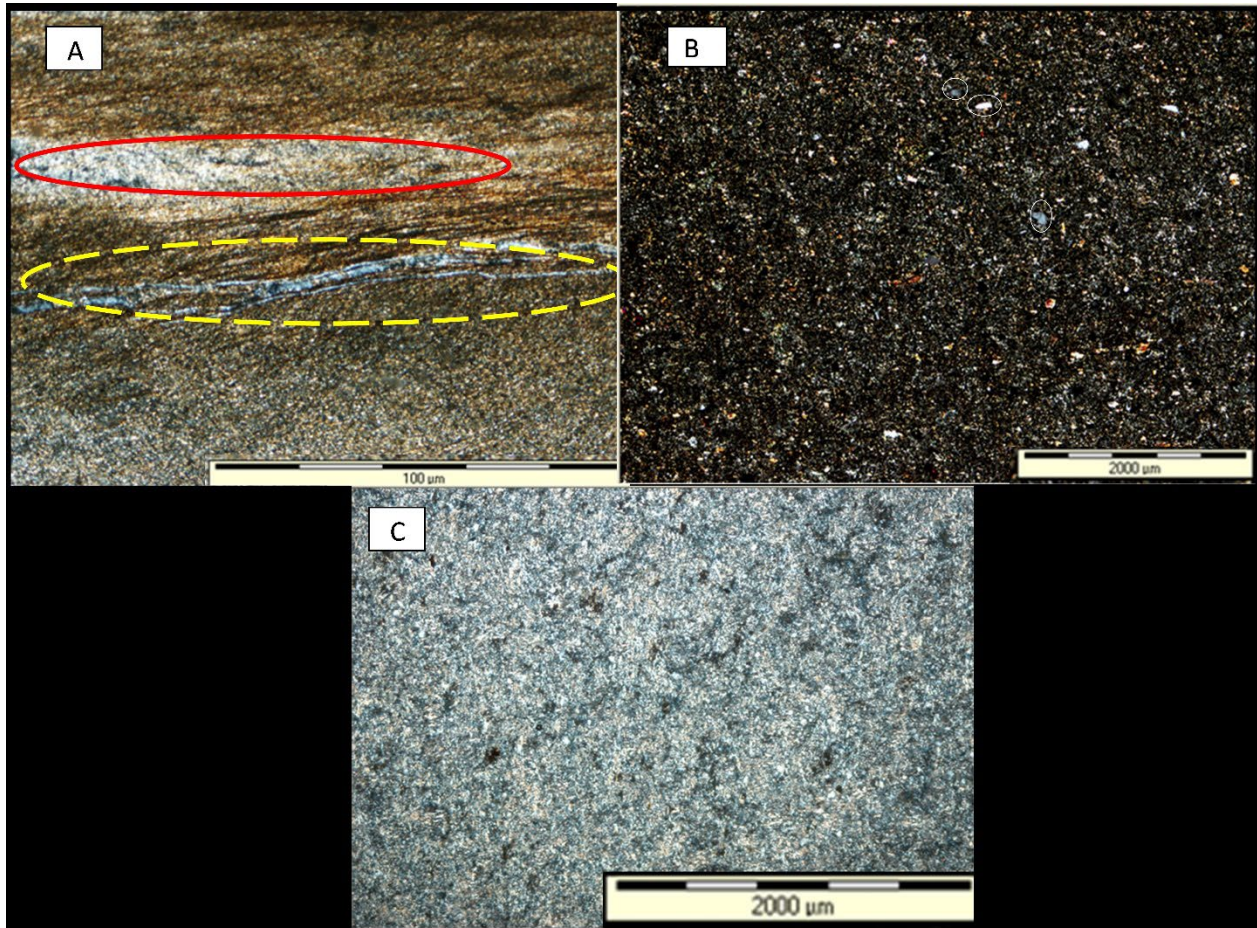


Figure 4. Photomicrographs of the shales of the Ecca Group: (A-B) Shale intercalated with siltstone; (C) Clay-rich mudstone

The black colour in Figure 4B may be the presence of opaque minerals that cannot be penetrated by light such as pyrite and oxides (ilmenite), and the carbon material (graphite or organic matter). While others such as plagioclase, pyroxene and amphibole are dark. Then quartz (in white) is black but has what is called undulose extinction, where the mineral behaves like a shadow, at one point it will remain black. However, when the stage is rotated it might turn grey and even white as shown in Figure B in white circles.

As such according to the data projected by the XRD, the samples from the Collingham Formation have a high concentration of quartz, varying between 30-32%. Followed by a high smectite concentration of about 23-28%, plagioclase 12-13% then 10-13% and mica 4-5%.

Most of the samples within the Collingham Formation clays (consisting of smectite, chlorite, and kaolinite), followed by quartz, later plagioclase, mica and lastly microcline. Then the Whitehill Formation is likely to have clays in high concentration (consisting of kaolinite 26-16%, chlorite 10-7%, with some not being detected), and smectite varying between 6-15%, followed by quartz (being between 32-23%), followed by plagioclase, mica, pyrite, and dolomite. Samples from the Prince Albert Formation also have clay having the highest concentration (consisting of smectite (30-33%), kaolinite (12-18%), chlorite (6-9%), and sericite (6-5%)), followed by quartz (25-26%), plagioclase (at 10-11%), and lastly mica (averaging 3%). As such it can be summarized that most samples picked from the Ecca Group are most likely going to have a high content of clay, quartz, plagioclase, and mica, which is consistent with what was observed from the geochemical data of the trace and major elements.

5.2. Major elements

The reason for the analysis of the major elements, such as the oxides is they give the distribution patterns that give an idealised version of the mineralogy of the samples at hand. When analysing the results, the silica content is a bit low (average of 58.7 %), suggesting that the shales are from a silica-poor source. Furthermore, the aluminium content is also low with them being within the range of 14-19 %. However, there are about 3 samples which have percentages ranging from 28-30 %. This along with the idea that they have a potassium oxide that is at an average of 3.85, which can be taken as being high, considering the positive correlation depicted by the plot of K/Al, then one could take this as a sign of the high content of minerals that have a high potassium content. Such as micas, and potassium feldspars [19]. The author further added that the positive correlation mentioned before may mean the concentration of the potassium-bearing minerals may influence the aluminium content, meaning their concentration may be attributed to the presence of clay minerals.

In Figure 5 several plots were made by the abundance of Al_2O_3 being used as the normalizing entity when making comparisons among the different stratigraphic lithologies because these are observed to be immobile during processes such as metamorphism, weathering, and diagenesis [6]. The major elements in the shales suggested a positive correlation in K_2O and a negative correlation observed in the graphs of P_2O_5 , MgO , CaO , TiO_2 , Fe_2O_3 , Na_2O , and SiO_2 . As opposed to previous studies conducted by other researchers such as [6] who suggested that normally shales show a positive correlation in oxides versus Al_2O_3 such as in TiO_2 , MgO , K_2O and Fe_2O_3 , while in these results the only positive correlation is observed in K_2O . The author further explained that no trend would be observed in all the other oxides, while here there is only one graph depicting no trend, which is the graph of MnO .

5.3. Elemental depiction of oxides

The binary plots in Figure 6 are normalized by UCC, representing the Tierberg Formation, which shows enrichment of iron oxide and potassium oxide and with a few of the data being enriched in manganese oxide and phosphorus oxide while some of the data being depleted for both. The depletion which is consistent with this data is calcium oxide and titanium oxide. While the Collingham Formation is observed to have a single data, which tends to stand out, it is consistent with the rest of the samples. There is an enrichment in potassium oxide and iron oxide. There is an enrichment of aluminium oxide and iron oxide for the Collingham Formation with a depletion in some of the data of the Collingham Formation for iron oxide. With a depletion of calcium oxide, titanium oxide and phosphorous oxide for the Prince Albert Formation. As such the sodium depletion could be associated with a low concentration of sodium-rich plagioclase and this can be supported by the ratio of the K/Na which is greater than one. Suggesting that the potassium content is higher than the plagioclase.

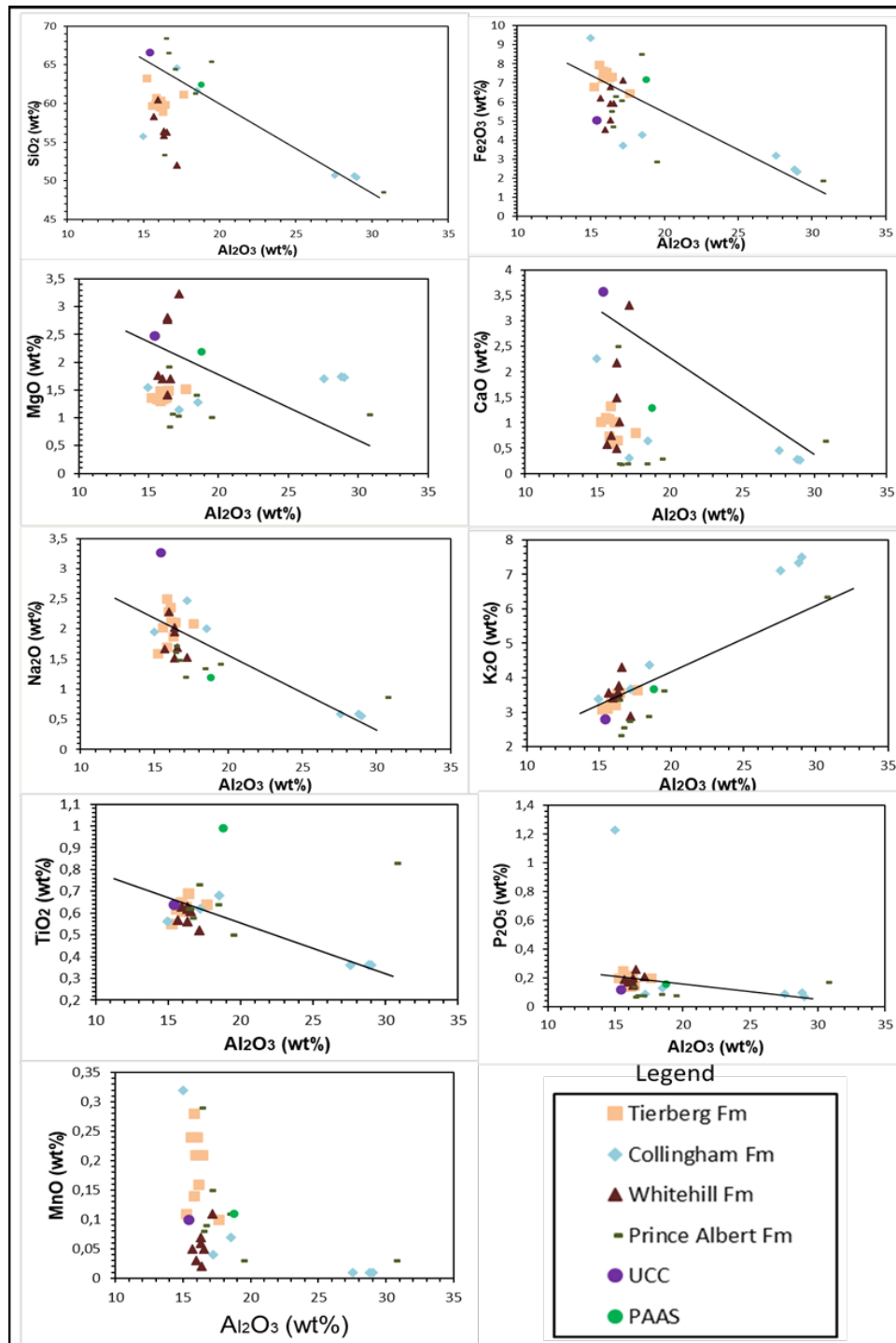


Figure 5. Relationship of the major elements versus Al_2O_3 along with their respective UCC and PAAS values for comparison by [16-17] respectively

For the PAAS normalized data, Figure 7 there is an enrichment of sodium oxide, and iron oxide with a few of the data being enriched while some are depleted in phosphorus oxide and manganese oxide. A depletion is observed with magnesium oxide, calcium oxide, and titanium oxide. In the Whitehill Formation, there is an enrichment of phosphorus oxide, and sodium oxide, with a single set of data being enriched with calcium oxide, with the other 3 being depleted in calcium oxide and titanium oxide. In the plot of Collingham Formation, there is an

enrichment in phosphorus oxide, potassium oxide, and aluminium oxide. While there is an observation of a few data sets being depleted and enriched with sodium oxide and iron oxide for the Collingham Formation. For Prince Albert Formation there is an enrichment of aluminium oxide, iron oxide, sodium oxide, and a depletion of calcium oxide (with one set being enriched in the same calcium oxide), and iron oxide (with a few sets of data being depleted in iron oxide), phosphorus oxide (a depletion of phosphorus oxide was depleted).

The enrichment in CaO is normally associated with the presence of calcite cement which may have during diagenetic processes [6]. While in this research for both UCC and PAAS compared spider plots, there is a depletion in calcium oxide, suggesting that the diagenetic conditions were not as persistent as those found on the Eastern side. It was observed that amongst the oxides aluminium and silica ratios tend to be sensitive to sedimentary recycling and weathering processes, meaning they can suggest sedimentary maturity along with their provenance of origin. It was suggested that if the average of the silica to aluminium ratio is at 3-5, then it is from a basic source, but when it is at 5> then it is from an acidic source. As such the silica average is at 56.68%, while the aluminium is at 18.19%, giving a Si/Al ratio of 3.1, according to the data provided the shales are from a basic source. Another author suggested that the ratio of K/Na normally does not exceed 0.3, with those reaching 0.6 having been altered [18].

As such the ratio of Na/K is found to be at 0.4, which is above the range of 0.3, suggesting that the samples have been altered. Additionally, they suggested that when the Mg# (magnesium number) value is calculated using $Mg / (Fe + Mg) * 100$, then the sum of the average must be approximately 44% for a mafic rock. Furthermore, the Mg# (magnesium number) of the results is at 23%, which may be consistent with intermediate origin. In addition, the average silica content of the samples is 58.7 %, which is also consistent with that of intermediate origin as suggested by [18]. Similarly, the data in this study and that of previous studies oppose each other. Except when the manganese oxide and potassium oxide result. Which suggests an enrichment in clay material.

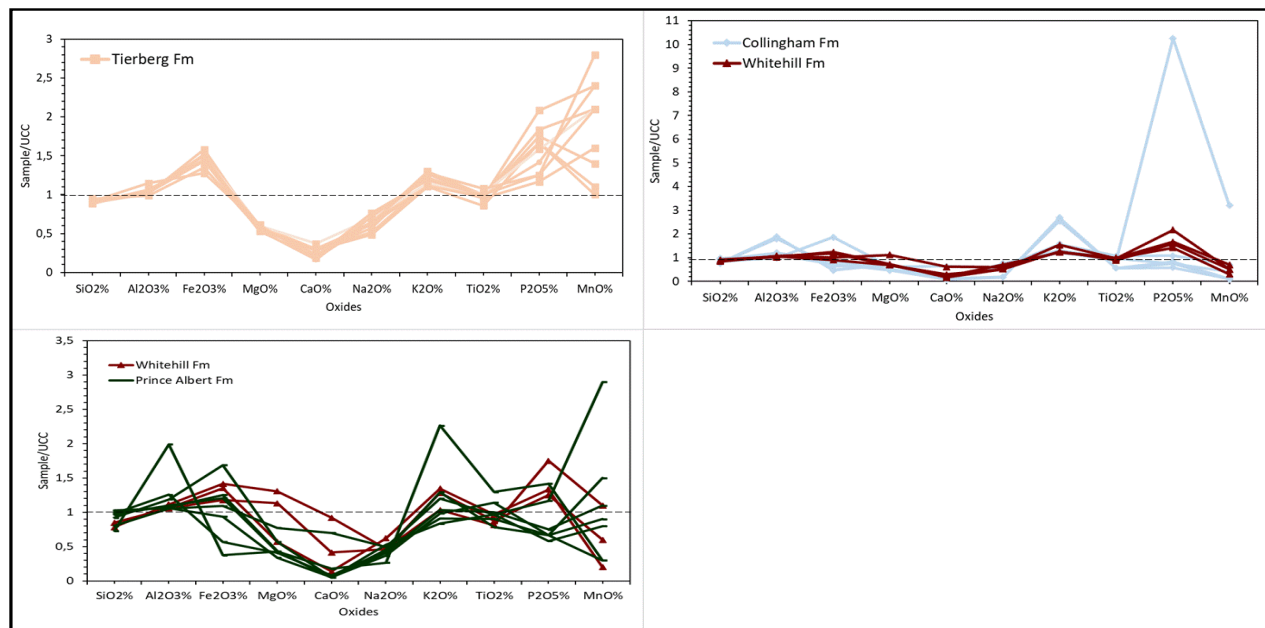


Figure 6. Representation of major elements which have been normalized using the UCC value by [16]

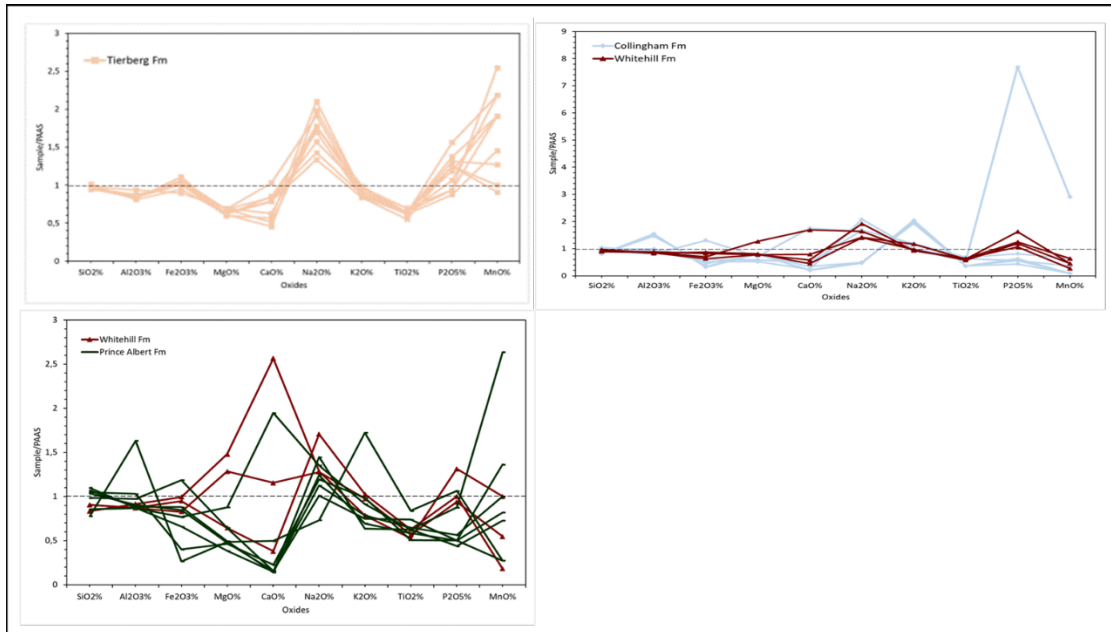


Figure 7. Representation of major elements which have been normalized using the PAAS value by [17]

5.4. Elemental depiction of trace elements

In Figure 8, it has been noticed that the trace element concentration is anomalous or shows the highest peaks within the LILE compartment, especially the Collingham Formation. The shale seems to be enriched in uranium (U), followed by thorium (Th), rubidium (Rb), and yttrium (Y) from the HFSE portion, with a single sample from the Collingham Formation also suggesting an enrichment in zircon (Zr) and gallium (Ga) and lastly, the TTE portion showing an enrichment on copper (Cu) and zinc (Zn).

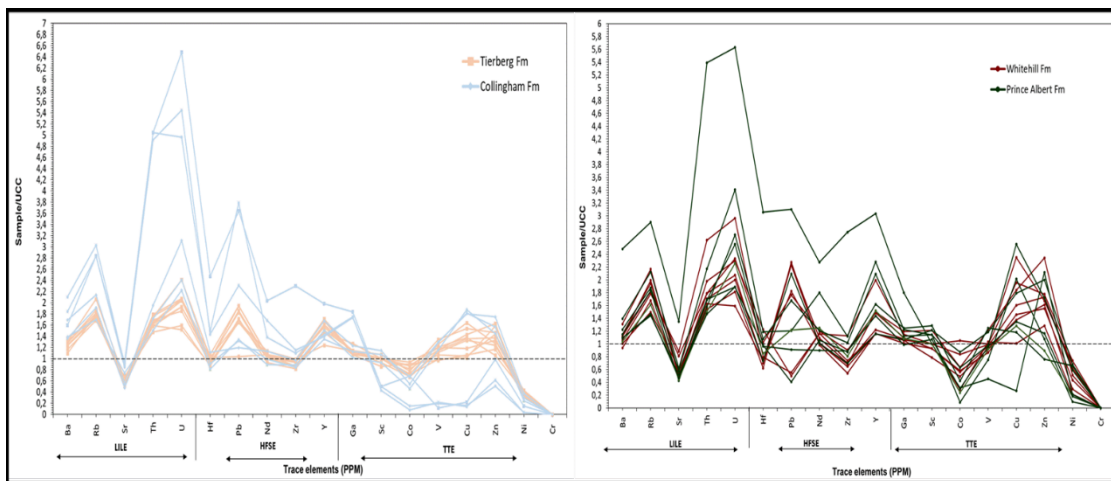


Figure 8. Representation of trace elements which are normalized using the UCC value from [16]

While the highest depletion is from the two samples within the Collingham Formation in the TTE portion of the graph, suggesting a depletion in cobalt (Co), vanadium (V) and copper (Cu). On the very same TTE, the samples correspond with each other as a depletion in chromium (Cr) and nickel (Ni) is observed, followed by cobalt (Co), and then zircon (Zr) from the HFSE. Then followed by sharp peaks also suggesting a depletion from strontium (Sr) and lastly hafnium (Hf). For the Prince Albert Formation, a similar trend is observed, but a bit exaggerated when compared to the others, these range from a slight increase in vanadium (V) concentration. Most of the samples correspond with each other namely an extreme depletion in chromium, nickel,

cobalt, lead (Pb), strontium and hafnium. While there is an enrichment in uranium, thorium, copper, zinc, yttrium, rubidium, neodymium (Nd) and scandium (Sc) in a decreasing fashion.

In Figure 9, a few of the samples in the Collingham Formation tend to be a bit more extreme as compared to the rest of the samples, with them suggesting an enrichment of elements such as uranium, lead, zircon and a major depletion in vanadium, cobalt, and copper. The rest of the samples show a uniformity of some sort with the enrichment being on elements such as uranium, lead and zinc in a decreasing fashion. With a depletion being observed in elements such as chromium, nickel, cobalt, neodymium, copper, and strontium. The plot of the Collingham Formation follows the same trend as the Prince Albert Formation with these huge peaks that stand out.

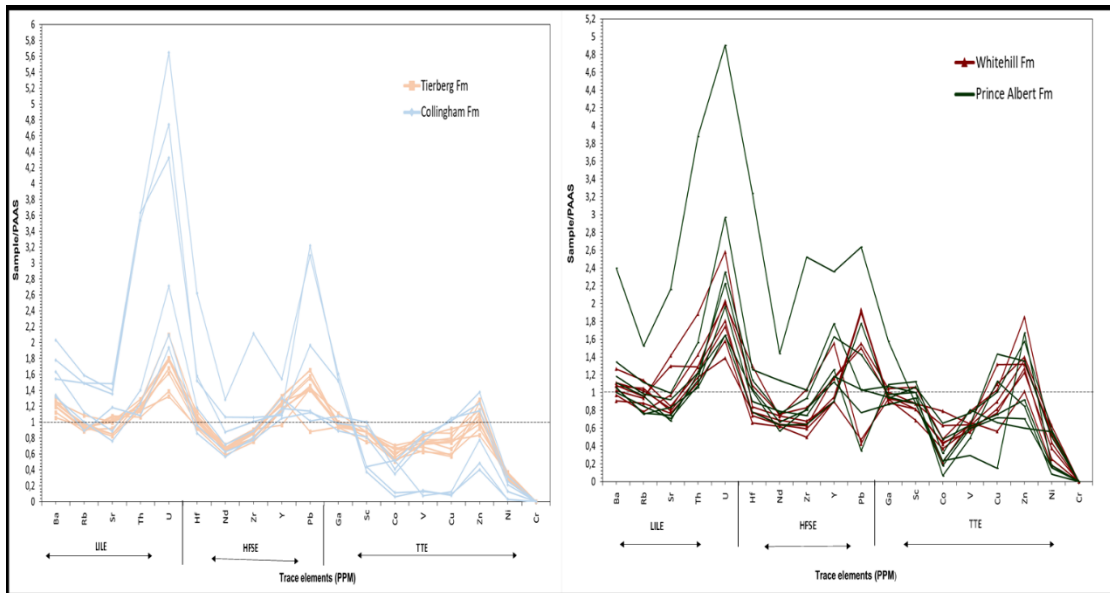


Figure 9. Representation of trace element normalized using the PAAS value from [17]

Authors such as [19-21] suggested that elements such as REE, Th and Sc are regarded as being reliable when being analysed since their presence is not affected by the heavy mineral fractionation as compared to other minerals such as Hf, Zr and Sn. Thorium enrichment and the low or negative anomalies presented by the Sc, Cr and Co suggest that these samples are within a felsic basin. Within this research when comparing the PAAS and UCC normalised graphs, there is a shift, in the sense that the V, Co and Cr are depleted while in the other there is an enrichment in V, which would point to a mafic source. This along with the high concentration of LILE and HFSE elements suggest a felsic source [19]. Again, the enrichment of both Zr and Sr may suggest an association of some sort with calcite material [6]. While in this research there is a depletion in both, which also supports the CaO depletion within the oxide portion.

[20] suggested that for a material to be seen as being from a mafic or intermediate source there would be a strong depletion in highly compatible materials such as Sr, P, and Ti, which can be observed in the graphs above. The presence of enrichment in Th and Nd may suggest that these minerals are controlled by clay material as for the likes of Ti and Nd bearing phase [6]. While in this study there is an observation of the enrichment of Th but a depletion of Nd. According to [20], using the Dniester Bug Series, the samples must be depleted in elements such as Cs, Rb, Th, U, and K (highly incompatible elements) except for Ba. The reason being during granulated facies metamorphism these elements can be mobile, hence their depletion does not represent the depletion from the source but a depletion that came about by being removed during metamorphism. According to [6] if a sample has a high positive enrichment in Zr and Hf, then the sample may mean that it is controlled by zircons, but in this study, there is a depletion in both elements suggesting that the sample was not controlled by zircons.

5.5. Provenance of the source rocks

The source rocks of the Ecca Group shales have been shown using the different discriminant binary diagrams which were plotted using the different major and trace element values from the XRF analysis, with one including Figure 10(a) which is a discriminant function 1 versus discriminant function 2. This diagram has been divided into four different quadrants with each representing a certain source. These are the intermediate igneous source, felsic igneous source, mafic igneous source and lastly quartzose sedimentary source. In this regard, about twelve of the samples have been found under the quartzose sedimentary source, while eighteen of the samples fall under the mafic igneous source.

Most of the samples plotted in the section of the mafic igneous rocks, with about eight of the samples being in the intermediate igneous rocks and one of the samples plotted under the felsic igneous rocks (Figure 10b). This is a binary plot represented by three divisions, the mafic portion, the felsic portion, and the intermediate igneous portion.

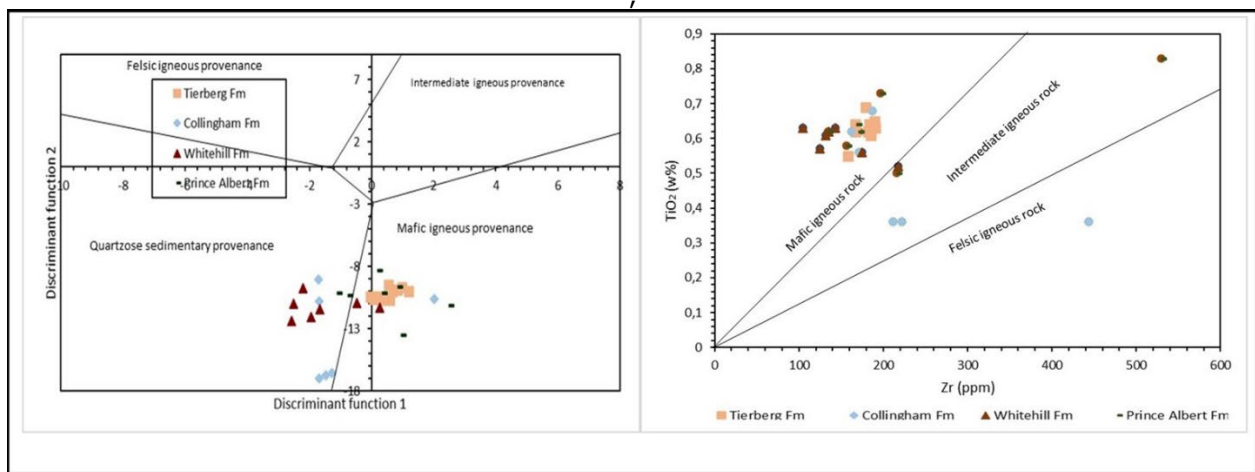


Figure 10. A is a presentation of a discriminant function for the provenance of the shale background from [35]. The discriminant functions are Discriminant Function 1 = $(-1.773 \text{ TiO}_2) + (0.607 \text{ Al}_2\text{O}_3) + (0.760 \text{ Fe}_2\text{O}_3) + (-1.500 \text{ MgO}) + (0.616 \text{ CaO}) + (0.509 \text{ Na}_2\text{O}) + (-1.224 \text{ K}_2\text{O}) + (-9.090)$; Discriminant Function 2 = $(0.445 \text{ TiO}_2) + (0.070 \text{ Al}_2\text{O}_3) + (-0.250 \text{ Fe}_2\text{O}_3) + (-1.142 \text{ MgO}) + (0.438 \text{ CaO}) + (1.475 \text{ Na}_2\text{O}) + (-1.426 \text{ K}_2\text{O}) + (-6.861)$. B is a presentation of Zr ppm versus TiO_2 wt. % of the shales background after [20]

While Figure 11(a) suggests that the data is from a passive margin source, the results are plotted in the passive margin portion, perhaps suggesting a calm condition in which the sediments were deposited. Hence, in turn, supporting why the stratigraphic column fine-grained materials, even the sand is very fine-grained. This is because calm conditions deposit material by the main suspension, meaning the water velocity is too low to be able to support the weight of heavy, large clasts.

Agreeing with the suggestion is Figure 11(b), a ternary diagram of V-Ni-Th*100 that has been plotted, showing that most of the data were nucleated near V (vanadium), which suggests that the data is of a mafic origin, while four of the samples from Prince Albert (1) and Collingham (3) formations suggest a felsic environment since the data is observed nearer to thorium. This makes sense as the plots near the vanadium are likely to have a composition of +/- 80% of V, and +/- 10% for each nickel and thorium, suggesting a mafic source.

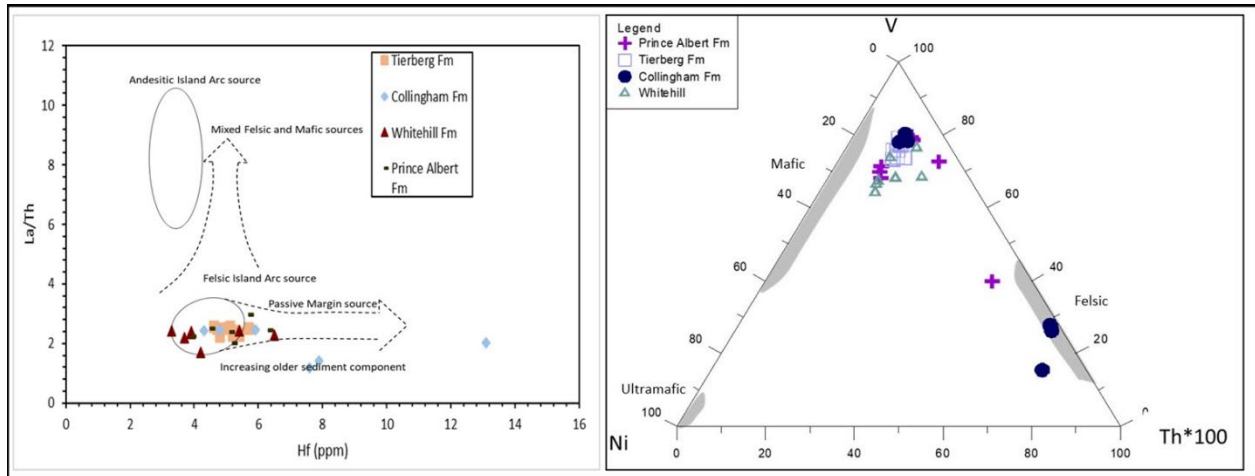


Figure 11. A is a representation of Hf versus La/Th for the shales after [21] and B is a representation of the V-Ni-Th*100 triangle diagram for the shales after [22]

Then a binary plot in Figure 12 is divided into 3 segments, which are a representation of Early Archean, Late Archean, and Post Archean. The results of the Eccca Group shales are plotted in the Post Archean time. Where "post," suggests after the Archean aeon has passed. This is consistent with the literature review, which suggests that the Main Karoo Basin was deposited in the Late Carboniferous to Mid-Jurassic. This period is found within the Phanerozoic Eon, within the Late Palaeozoic to Late Mesozoic Era according to the geologic time scale.

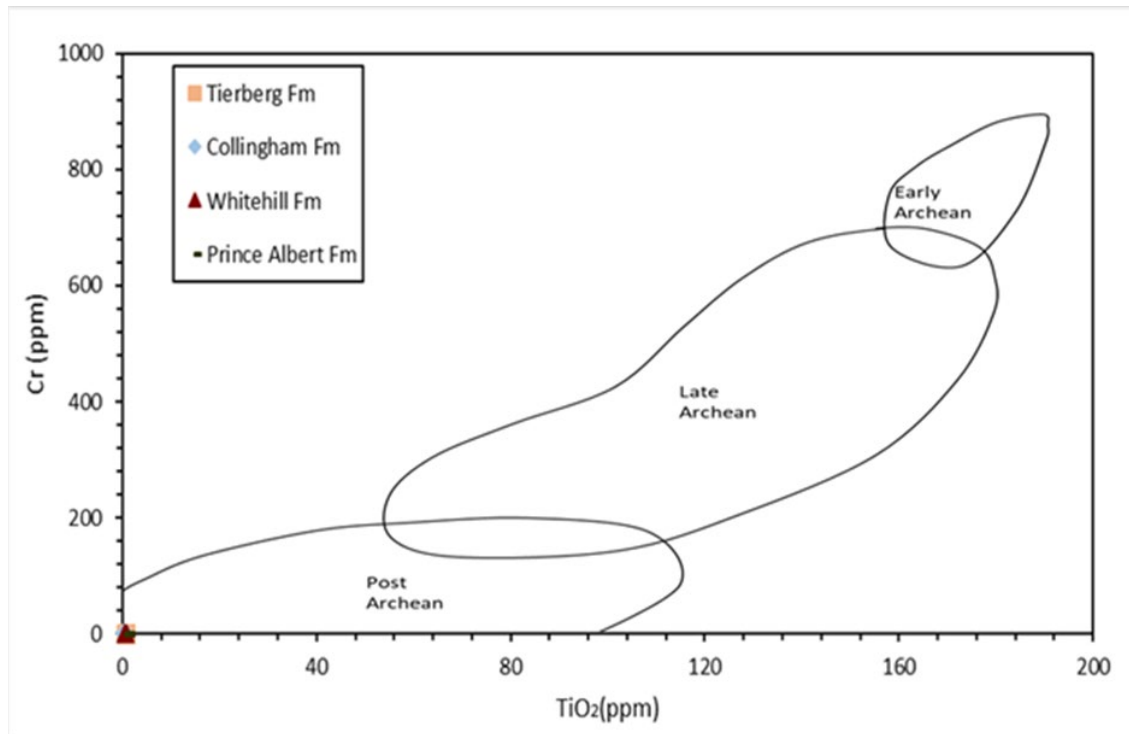


Figure 12. A binary plot of Cr versus Ti for the shale samples from the Eccca Group [23]. The samples are plotted close to the boundary (bottom left) of the post-Archean field

The plots represented in this section support are in favour of each other, hence creating an image of the data coming from a mafic source. The present quartzose sedimentary provenance, felsic and intermediate plotted points, may be due to several factors. Namely, the particles could have possibly been from different sources, transported, and later deposited

together within the basin. Ultra-mafic and mafic materials tend to react negatively when exposed to the elements of the atmosphere. Meaning because of the mountain build-up, which was occurring, there is a possibility that mafic material was exposed to the surface. As such it may have reacted to the water within the basin and later with the arid environment which may have weakened and weathered the rock, forming fine-grained material. Which also may support the formation of so much clay material. This may further be supported by the few sand materials found in the stratigraphy. Meaning felsic materials such as silica-rich material, tend to be a bit coarser-grained and a lot more resistant to the elements unless they have been worked and reworked.

One of the crucial factors noted during the analysis was the milling pot and crushing equipment must be thoroughly cleaned before each sample can be placed in, hence due to human errors. According to earlier studies, the shales of the Ecca Group are regarded as coming from a felsic source or provenance, while this study suggests mafic. This may be the case because when a rock is exposed to heat, water, and other elements, it is weathered down. This means the incompatible elements are more likely to leave, while elevated temperature minerals become uncomfortable or unstable and convert to the next stable material.

5.6. Tectonic setting of the source area

Several researchers [20,26-28] over the years have used binary plots to try and characterise the chemical composition of siliciclastic sedimentary rocks according to their provenance, tectonic settings, and depositional environments. As their chemical attributes are controlled by such factors. And in this case, it has been noted that when the sediments have not been strongly affected by post-depositional weathering and metamorphic processes, they have the potential to give reliable results. The binary plots depicted here are divided into 4 main settings, passive margin (PM), active continental margin (ACM), continental island arc (CIA), and oceanic island arc (OIA).

A passive margin is seen as the transition between oceanic and continental crust, meaning it is associated with a divergent plate boundary, suggesting that there are a few earthquakes with no volcanism [24]. Additionally, an active continental margin is characterised by a lot of volcanism and trenches, which is consistent with a convergent plate boundary. A continental island arc is associated with the subduction of an oceanic plate under another oceanic plate, while a continental island arc is associated with the subduction of an oceanic crust below a continental crust [25].

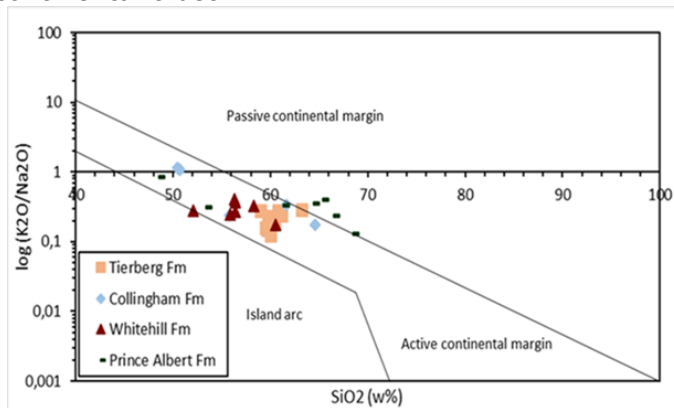


Figure 13. A binary plot of K_2O/Na_2O versus SiO_2 tectonic-setting discrimination diagram for Ecca Group shales, background field after [26]

In the binary plot in Figure 13, the divisions of the graph are 3, namely the OIA, ACM, and PM. Much of the data is noted to be in the PM with a minor of the data being in the ACM. Then there are 3 ternary plots are plotted consisting of the same tectonic setting as those found in the binary plots, in Figure 14(a), most of the data is found in the PM and minor data points in the ACM. Lastly, Figure 14(b) has all the data points in a part that combines the PM and the ACM. As such a common trend that has been seen in the graphs is that the tectonic setting source area is that of ACM and PM.

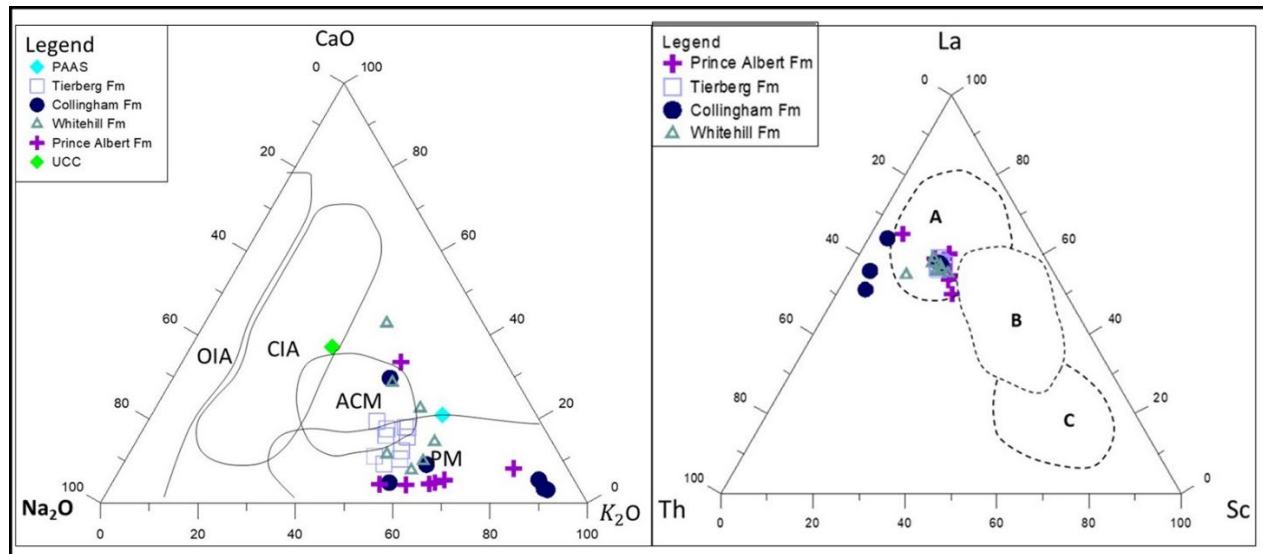


Figure 14. A is a representation of the Na_2O - CaO - K_2O ternary plot for the shale background field after [27]. OIA = Oceanic Island Arc, CIA = Continental Island Arc, ACM = Active Continental Margin, PM = Passive Continental Margin. B is a representation of the La-Th-Sc tectonic discrimination diagram for the Ecca shales, background after [28]. A = Passive and Active Continental Margin, B = Continental Island Arc, C = Oceanic Island Arc.

5.7. Paleoweathering conditions

The amount of chemical weathering that takes place in a basin is mainly dependent on factors such as the source rock, if they are ultramafic, they are likely to be altered at a quicker pace as opposed to when they are felsic. The time in which they are exposed to the elements, the climatic conditions, and the rate of tectonic uplift [6]. The author suggested that most of the material that forms the upper crust is mainly feldspar and volcanic glass, which further suggests that when the material is subjected to chemical weathering, it will be converted into clay material. Meaning elements such as Ca, K, and Na are likely to be removed, with the minor ones being left suggesting evidence of intense weathering [29].

Another author added that results from alkali material ($\text{Na}_2\text{O} + \text{K}_2\text{O}$) and K/Na siliciclastic material should be considered reliable indicators of the intensity of weathering if they have been free of alkali-related post-depositional modifications [6]. As such if the ratio of K/Na is below 0.3 then it is not altered, but if it is above 0.3-0.6, then it is altered, as is seen in this research (shown by 0.4).

The binary plots exhibited in Figure 15 of $\text{K}_2\text{O}/\text{Na}_2\text{O}$, $\text{K}_2\text{O} + \text{Na}_2\text{O}$, Na_2O , K_2O and CaO against PIA, are used to infer information about the mobility of elements during the late stages of weathering. The first one suggests that the ratio between the two increases with an increase in PIA, in the second one the opposite is true, meaning as the value of PIA increases the content of the two decreases. In this research, weathering and alteration indices such as the chemical index of weathering ranging between 78-96% with an average of 87%, the chemical index of alteration ranging between 66-81% at an average of 74%, the plagioclase index of alteration ranging between 73-76%, averaging at 75% and index of compositional variability that ranges between 0.3-1.25% averaging at 0.8%. [30] suggested that if the CIA value is above 80%, then the samples are strongly chemically weathered, if it ranges between 80-60%, then they are moderately chemically weathered from the source but if it is below 60% then it means they have been initially weathered from the source area. In this research the samples had a CIA value which was between 80-60% (75%), suggesting chemical weathering of these samples was moderate. In this research, the PIA average is observed to be at 75% which suggests that the samples underwent high weathering in the source area.

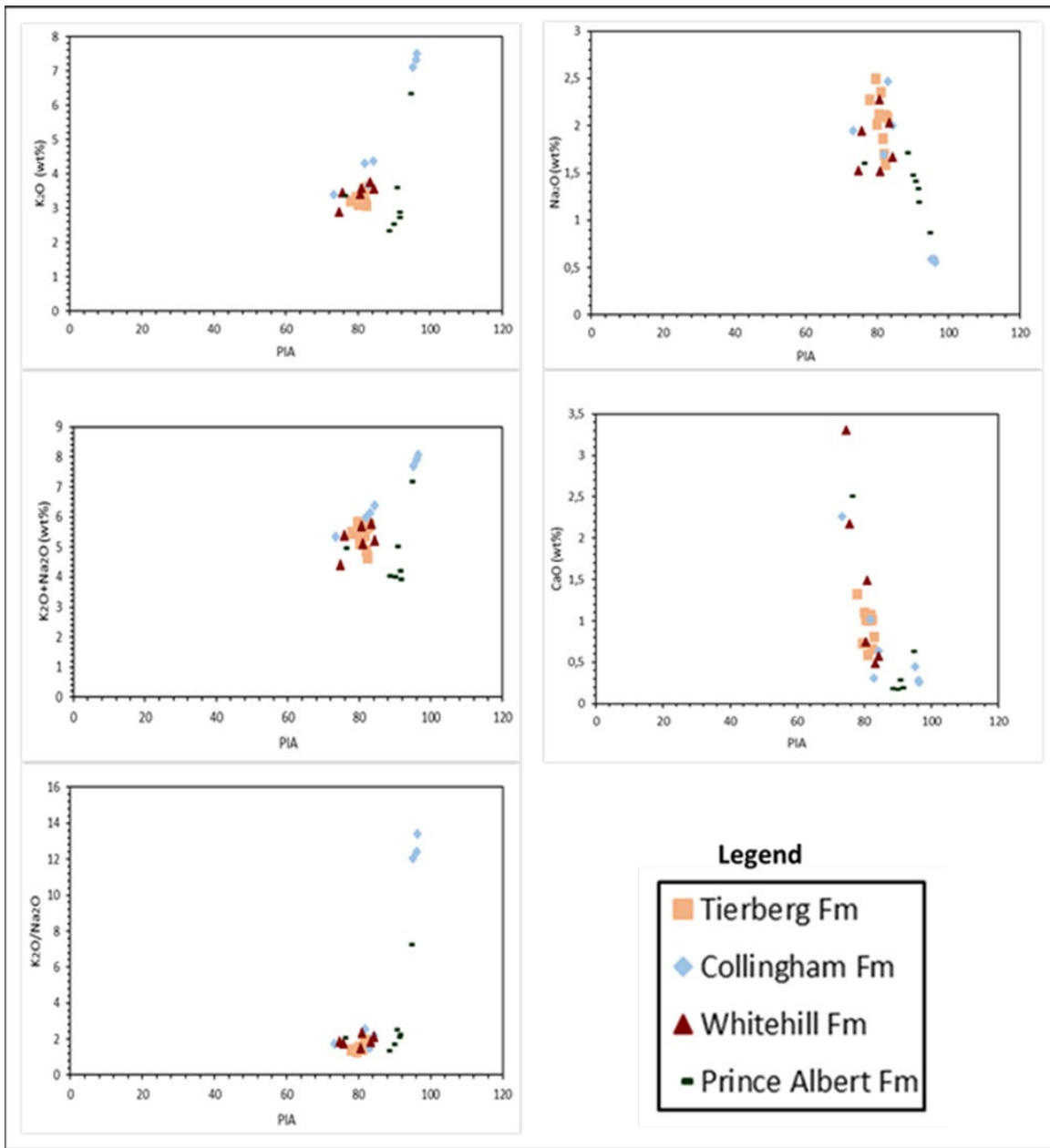


Figure 15. A Bivariate diagram depicting the mobility of elements during weathering of feldspars in shale samples from the Eccca Group. (K_2O/Na_2O_3) wt. % versus PIA. ($K_2O + Na_2O$) wt. % versus PIA. Na_2O wt. % versus PIA. CaO wt. % versus PIA. K_2O wt. % versus PIA

In Figure 16, a ternary plot depicts and assesses the composition of origin and the mobility of elements when undergoing the process of chemical weathering. The ternary plot consists of 5 arrows, which represent the weathering trend of gabbro (1), tonalite (2), granodiorite (3), adamellite (4), and granite (5). Most of the data is nucleated on arrow 4, with some being presented in front of arrow 3. There is also a red dotted arrow which moves parallel to the A-CN portion of the graph, which may show the greater rate at which sodium and calcium are removed from plagioclase concerning the potassium. This along with the trend toward illite without any inclination to the apex of potassium simply means that there was no potash metasomatism during diagenetic processes. Hence, the plot suggests that weathering conditions are consistent with the rate at which material is removed.

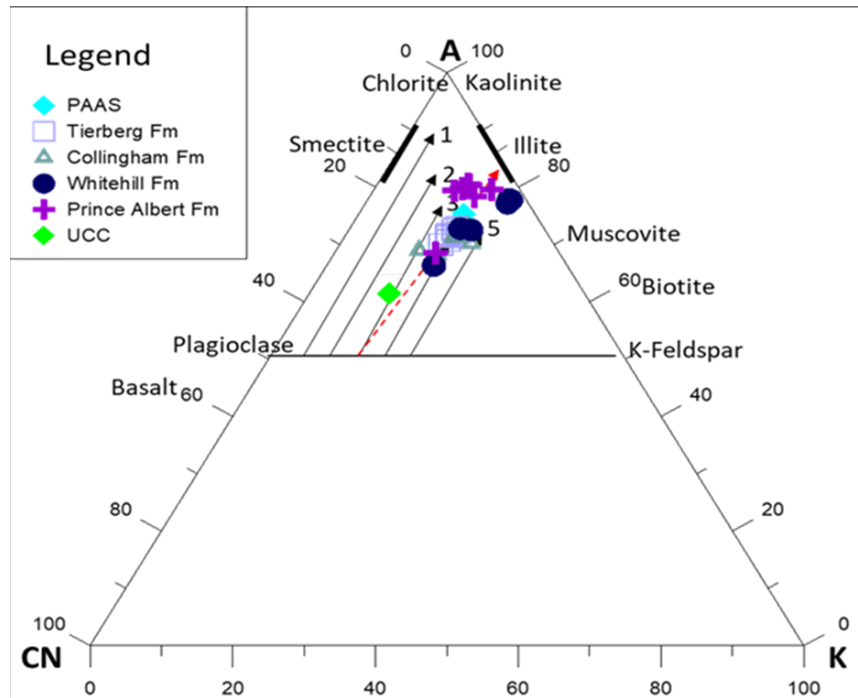


Figure 16. A-CN-K ternary diagram of molecular proportions of $Al_2O_3-(CaO+Na_2O)-K_2O$ for shales from the Ecca Group [31]. The dotted arrow shows the actual weathering pattern for the samples. The CIA scale shown on the left side is for comparison

5.8. Paleoclimatic conditions and sediment maturity

In Figure 17(a), there is a binary plot of ICV versus CIA, within this plot, there are three divisions the mature, intensive weathering, and the immature segment to the left. Meaning if the $ICV > 1$, then the sediments are compositionally immature, which suggests that the sediments were preserved in tectonically active conditions. While if it is < 1 then it is mature and was deposited in a tectonically calm or cratonic environment. To determine the maturity and character origin of the shales, the ICV was calculated. It has also been found that minerals that have a high weathering intensity tend to have a high ICV, which further adds that this will create a decrease in more stable minerals [32].

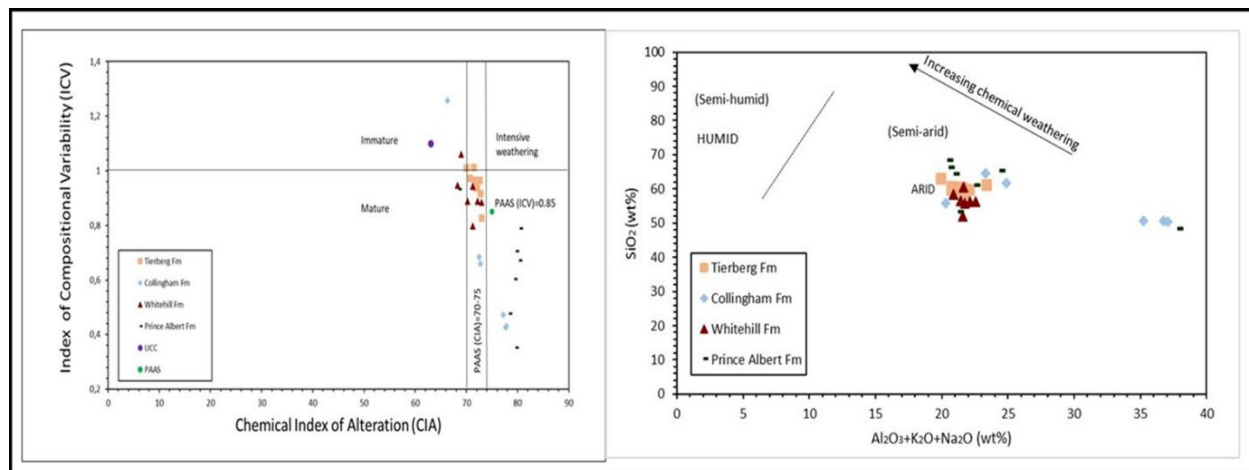


Figure 17. Binary plot of CIA against ICV for the Ecca shales on a background diagram of [32]. An equation for calculating ICV is $ICV = (Fe_2O_3 + K_2O + Na_2O + CaO + MgO + MnO) / Al_2O_3$. While B is a representation of the chemical maturity of the Ecca Group and shales background after [33]

Most of the data is plotted within the mature segment of the plot near the PAAS, while 3 to 4 of these data are within the immature section. This implies that the data shows a transition from the immature to mature section as the data progresses to move to the right within the intense weathering portion of the graph. While Figure 17(b) shows the maturity of the shales concerning the climate. Most of the data is plotted within the arid segment of the graph along with a few on the far right of them suggesting an increase in chemical weathering. It was observed that when the average ratio of Si/Al is >5.0 , suggesting that the shales are progressively mature [33]. Since the Si/Al ratio of the data is 3.1 then they concur. Another author suggested that if the CIA value is between 76-100%, then that simply meant that the samples indicate a high chemical weathering in the source area, while a value that is $<50\%$, suggests a low to no chemical alteration [29]. In this case, the CIA value ranges from 66- 81% at an average of 74%, suggesting that the samples have undergone intensive chemical weathering in the source area. These findings are consistent with those found by other authors.

6. Conclusions

The provenance, tectonic setting and paleoweathering conditions of the Permian shales of the Ecca Group in the Main Karoo Basin has been assessed using inorganic geochemical studies. The major oxide and trace element concentrations in the shales show significant variation in composition across the samples. Higher concentration of Al_2O_3 , Fe_2O_3 , K_2O , Sc, V, Zr, Th, U, La, Ce, and Ni are observed in the shales. The preferential enrichment of transitional elements like Sc, V, and Ni in the shales is probably due to surficial sorption. Furthermore, the low concentration of these elements, La/Sc and Th/Sc ratios suggest the presence of fractionated source rocks with lower compatible element contents and recycled sediments in the source area. Likewise, the discrimination diagrams based on major oxide geochemistry shows that the shales are mainly of quartzose sedimentary provenance with little contribution from the mafic igneous provenance, suggesting that they were mostly derived from a cratonic interior or recycled orogen. The tectonic setting discrimination diagrams support active-passive continental margin setting of the provenance. In addition, the CIA and PIA values, as well as the bivariate plots of ICV versus CIA, and SiO_2 against total alkali ($Al_2O_3+K_2O+Na_2O$) suggest that the source area of the shales were subjected to intense weathering conditions under arid climate.

References

- [1] Johnson MR, van Vuuren CJ, Hegenberger WF, Key R, and Show U. Stratigraphy of the Karoo Supergroup in Southern Africa: An overview. *Journal of Africa Earth Sciences*, 1996; 23 (1): 3-15.
- [2] Speight JG. -Origin of shale gas. *Shale gas production processes*, 2014; Chapter 1,1-23.
- [3] Scott SD. *Geochemistry of mineral deposits (Second edition)*. Treatise on geochemistry, 2014; 13: 23-25.
- [4] Armannsson H, Oskarsson F, and Fridriksson T. *Geochemical exploration techniques (Second edition)*. *Comprehensive renewable energy*, 2022; 7:80-97.
- [5] Cullers RL. The geochemistry of shales, siltstones and sandstones of Pennsylvanian-Permian age, Colorado, USA: implications for provenance and metamorphic studies. *Lithos*, 2000; 51:181-203.
- [6] Baiyegunhi C, Liu K, and Gwavava O. Geochemistry of sandstones and shales from the Ecca Group, Karoo Supergroup, in the Eastern Cape Province of South Africa: Implications for the provenance, weathering and tectonic setting. *Open geosciences*, 2017; 9(1):340-360.
- [7] Geel C, Schulz H.M, Booth P, de Wit M, and Horsfield B. Shale gas characteristics of the Permian black shales in South Africa: results from recent drilling in the Ecca Group (Eastern Cape). *Energy Procedia*, 2013; 40:256-265.
- [8] Bordy E, and Smithard T. The effects of dolerite intrusions on the hydrocarbon potential of the lower Permian Whitehill Formation (Karoo Supergroup) in South Africa and Southern Namibia: A preliminary study. *South African Journal of Geology*, 2015; 118(489):510-526.
- [9] Black DE, Booth PWK, and de Wit MJ. Petrographic, geochemical, and Petro-physical analysis of the Collingham Formation near Jansenville, Eastern Cape, South Africa- potential cap rocks to shale gas in the Karoo. *Geological Society of South Africa*, 2016; 119(1):171-186.

- [10] Baiyegunhi C, Nxantsiya Z, Pharoe K, Baiyegunhi T.L, and Mepaiyeda S. Petrographical and geophysical investigation of the Ecca Group between Fort Beaufort and Grahamstown, in the Eastern Cape Province, South Africa. *Open Geoscience*, 2019; 11(1): 313-326.
- [11] Smith RMH. A review of stratigraphy and sedimentary environments of the Karoo Basin of South Africa. *Journal of African earth sciences (and the middle east)*, 1990; 10(1-2):117-137.
- [12] Catuneanu O, Wopfner H, Eriksson PG, Cairncross B, Rubidge BS, Smith RMH, and Hancox PJ. The Karoo basins of South-central Africa. *Journal of African earth sciences*, 2005; 43(1-3):211-253.
- [13] Smith RHM, Eriksson PG, and Botha WJ. A review of stratigraphy and sedimentary environments of the Karoo Basin of South Africa. *Journal of African earth sciences (and the middle east)*, 1993; 16(1-2):143-169.
- [14] Keeditse M, Watanabe Y, Arribas A, and Buamono H. Diagenetic and epigenetic origins for Cu-Ag mineralization in the Khoemacau Zone 5 deposit, Kalahari Copperbelt, North-western Botswana. *Resource Geology*, 2022; 71(1):190-197.
- [15] Geel C, Nolte S, and Bordy E.M. Geochemical properties of the Permian black shales in the southern main Karoo Basin: lessons from compositional and petrophysical studies. *South African Journal of Geology*, 2021; 124(3):001-005.
- [16] Rudnick RL, and Gao S. Composition of the Continental Crust. In: Rudnick, R.L., Ed., *The Crust*, Elsevier-Pergamon, Oxford, 2003; 1-64.
- [17] Taylor SR, and McLennan, SM. *The Continental Crust: Its Composition and Evolution*. Blackwell Scientific Publications, 1985; 312-340.
- [18] Claesson S, Artemenko G, Bogdanova S, and Shumlyanskyy L. Archean crustal evolution in the Ukrainian Shield (Second edition). *Earth's oldest rocks*, 2019; Chapter 33, 837-854.
- [19] Anani C, Moradeyo M, Atta-Peters D, Kutu J, Asiedu D, and Boamah D. Geochemistry and provenance of sandstones from Anyaboni and surrounding areas in the Voltaian basin, Ghana. *International Research Journal of Geology and Mining*, 2013; 3(9):206-212.
- [20] Hayashi K, Fujisawa H, Holland H, and Ohmoto H. Geochemistry of ~1.9 Ga sedimentary rocks from north-eastern Labrador, Canada. *Geochemical et Cosmochimica Acta*, 1977; 61(19): 4115- 4137.
- [21] Bracciali L, Marroni M, Pandolfi L, and Rocchi S. Geochemistry and petrography of Western Tethys Cretaceous sedimentary covers (Corsica and Northern Apennines): From source area to configuration of margins, in Arribas, J., Critelli, S., Johanson, M.J., (eds.), *Sedimentary provenance and petrogenesis: Perspectives from petrography and geochemistry*. Geological Society of America, Special Paper, 2007; 42: 73-93.
- [22] Floyd PA, and Leveridge BE. The tectonic environment of the Devonian Gramscatho basin, south Cornwall: Framework mode and geochemical evidence from turbiditic sandstones. *Journal of the Geological Society London*, 1987; 144: 531-542.
- [23] Dipietro JA. Keys to the Interpretation of geological history. *Landscape Evolution in the United States*, 2013; Chapter 20, 327-344.
- [24] Hanif MA, Nadeem F, Tariq R, and Rashid U. Geothermal energy production. *Renewable and Alternative Energy Resources*, 2022; Chapter 8, 431-553.
- [25] McLennan SM, Hemming S, McDaniel DK, and Hanson GN. Geochemical approaches to sedimentation, provenance, and tectonics. In: M.J. Johnson and A. Basu, (Eds.), *Processes Controlling the Composition of Clastic Sediments*. Geological Society of American Special Paper, 1993; 32: 21-40.
- [26] Bhatia MR, and Crook KAW. Trace element characteristics of greywacke and tectonic setting discrimination of sedimentary basins. *Contributions to Mineralogy and Petrology*, 1986; 92: 181-193.
- [27] Cai Y, Ouyang F, Luo X, Zhang Z, Wen M, Luo X, and Tang R. Geochemical characteristics and constraints on provenance, tectonic setting and paleo weathering of the Middle Jurassic Zhiluo Formation sandstones in the Northwest Ordos Basin, North-Central China, 2022; 12:603.
- [28] Nesbitt HW, Fedo CM, and Young GM. Quartz and feldspar stability, steady and non-steady state weathering and petrogenesis of siliciclastic sands and muds. *Journal of Geology*, 1997; 105:173-191
- [29] Nesbitt HW, and Young GM. Prediction of some weathering trends of plutonic and volcanic rocks based upon thermodynamic and kinetic consideration. *Geochimica et Cosmochimica Acta*, 1984; 48: 1523-1534.

- [30] Roser BP, and Korsch RJ. Determination of tectonic setting of sandstone-mudstone suites using SiO₂ content and K₂O/Na₂O ratio. *Journal of Geology*, 1986; 94: 635-650.
- [31] Toulkeridis T, Clauer N, Kröner A, Reimer T, and Todt W. Characterization, provenance, and tectonic setting of Fig Tree greywackes from the Archaean Barberton Greenstone Belt, South Africa. *Sedimentary Geology*, 1999; 124: 113-129.
- [32] Cox R, Low DR, and Cullers RL. The influence of sediment recycling and basement composition on the evolution of mudrock chemistry in the southwestern United States. *Geochimica et Cosmochimica Acta*, 1995; 59(14): 2919-2940.
- [33] Suttner LJ, and Dutta PK. Alluvial sandstone composition and paleoclimate: I. Framework mineralogy. *Journal of Sedimentary Petrology*, 1986; 56: 329-345.
- [34] McAleer RJ, Jubb AM, Hackley PC, Walsh GJ, Merschat AJ, Regan SP, Burton WC, and Vazquez JA. Photoluminescence imaging of whole zircon grains on a petrographic microscope- An underused aide for geochronologic studies. *Minerals*, 2020; 10(10):876-889.
- [35] Roser BP, and Korsch RJ. Provenance signature of sandstone mudstone suite determined using discriminant function analysis of major element data. *Chemical Geology*, 1988; 67: 119-139.

To whom correspondence should be addressed: Tsibula J Sekantsi, Department of Geology and Mining, University of Limpopo, Private Bag X1106, Sovenga 0727, Limpopo Province, South Africa; e-mail: tsibulasekantsi@gmail.com